Cold Regions Science and Technology, 16 (1989) 167–174
Elsevier Science Publishers B.V., Amsterdam — Printed in The Netherlands

A BLOWING SNOW PARTICLE DETECTOR

T. Brown[1] and J.W. Pomeroy[2]*
[1]*Division of Hydrology, College of Engineering, University of Saskatchewan, Saskatoon, Sask. S7N 0W0 (Canada)*
[2]*School of Environmental Sciences, University of East Anglia, Norwich NR4 7TJ (U.K.)*

(Received June 20, 1988; revised and accepted August 29, 1988)

ABSTRACT

This blowing snow particle detector (PD) operates at temperatures from above freezing to −40°C and samples the range of blowing snow particle fluxes found from within 0.01 m of the snow surface to several metres height. It has a small sampling area, presents minimal interference with atmospheric flow, can be interfaced to an automated data retrieval system and requires only limited field maintenance.

The PD utilizes a 20 mm long, 170 μm radius beam of near-infrared radiation to sense the presence of blowing snow particles. It detects snow particles with radii as small as 22.5 μm and velocities of the full range expected for atmospheric flow in the Earth's boundary-layer.

Using Mie electromagnetic scattering theory, knowledge of the interception geometry formed by a snow particle and the beam and estimates of the snow particle size frequency distribution, a simple technique for calculating the blowing snow flux is developed and tested.

INTRODUCTION

On the Canadian Prairies and in other cold, windswept regions, wind transport of snow occurs frequently and the resulting distribution of surface snow is highly irregular. The pattern and magnitude of the redistributed snow is important to agriculture, flood control, wildlife management, highway maintenance and the development of recreational areas. An understanding of the transport of snow by the wind is necessary to predict snow-cover distribution patterns. Development of suitable instrumentation to monitor snow transport in the field will enhance research on the process.

Schmidt (1977, 1984) and Gubler (1981) describe gauges which count individual blowing snow particles, based upon the number of interruptions to the transmittance of a narrow light beam as particles pass through the beam. As well, Schmidt's gauge estimates particle velocities and the size of individual particles. Interpreting the measurements of these gauges is an uncertain task, due to incomplete interception of the particle by the beam and non-uniform beam intensity (Schmidt, 1977; Gubler, 1981). Schmidt's gauge requires an intricate signal analysis, thus its response time is insufficient to sample snow flows with high particle number densities. A comparison of Schmidt's 1977 and 1984 gauges, Gubler's gauge and a mechanical snow trap (reported in Schmidt et al., 1984) shows notable differences in the estimated mass flux. As these devices are calibrated empirically, a standard measurement cannot be defined.

The blowing snow particle detector (PD) described herein overcomes the problems outlined above by monitoring the number of blowing snow particles using a smaller, faster and more sensitive photo-detector, and a light emitting diode (LED) for greater gauge stability. The uniform sensitivity of the PD measuring area makes signal processing faster and simpler. A theoretical procedure calculates the mass flux from the PD output and corrects

*Permanent Affiliation: Rocky Mountain Forest and Range Experiment Station, U.S. Forest Service, Department of Agriculture, 222 South 22nd Street, Laramie, WY 82070-5299, U.S.A.

0165-232X/89/$03.50

for incomplete interception of snow particles by the detection beam, assuming the particles are members of a known size frequency distribution.

GAUGE DESCRIPTION

The PD counts the number of blowing snow particles which interrupt the transmission of a near-infrared beam of radiation. Interruptions of the beam causing the transmittance to drop below a threshold value register as particle counts.

The PD is shown in Fig. 1. It consists of left- and right-hand components mounted on a rectangular-shaped frame made of 6.4 mm thick, flat mild steel. The LED, located on the left-hand side, projects a narrow beam of radiation which is monitored by a photo-detector mounted on the right-hand side. An image conduit in front of the photo-detector permits the placement of the physical bulk of the PD electronic enclosure away from the measuring area. The beam, during 20 mm of its passage between exiting the LED and entering the image conduit, is subject to being interrupted by the flux of snow particles.

The gauge is orientated during operation, so that the flow of snow is perpendicular to the beam and normal to the plane of Fig. 1. The mounting bracket can be either on the top or the bottom, depending on the height of measurement. Flow visualization accomplished by observing the passage of snow particles through the gauge and examination of snow-dunes accumulated around the gauge, indicate the PD does not present an obstruction to the snow-air flow.

The optical components are the LED (Motorola MFOE1202[1]), with a peak emission wavelength of 820 nm and an effective radius of about 150 μm, and the photo-detector (Motorola MFOD2404[1]), an integrated detector/preamplifier (IDP) with a matching high response at 820 nm. The LED is selected for its narrow angular response. A 150 μm radius pinhole, placed in the radiation path of the photo-detector, limits the radiation reaching the photo-detector to approximately the same area as the LED.

The image conduit transmits a coherent image of the pinhole to the photo-detector. The 80 lines/mm resolution of the image conduit ensures maximum

[1]The use of trade and company name is for the benefit of the reader; such use does not constitute an official endorsement or approval of any service or product by the U.S. Department of Agriculture to the exclusion of others that may be suitable.

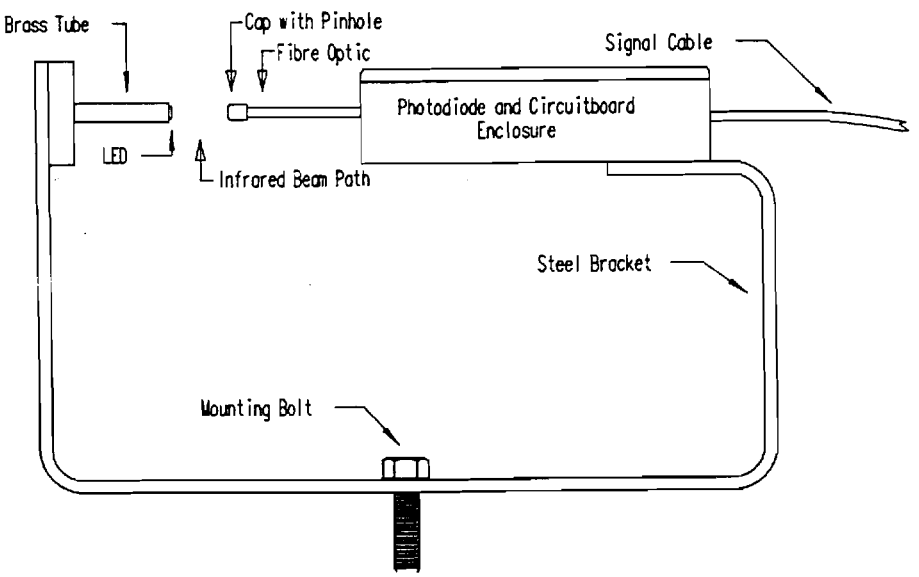

Fig. 1. Cross-sectional view of the particle detector. Dimensions are 230 mm long, 125 mm high with a gap of 20 mm between the LED and the fibre optic.

optical coupling of the image to the small active area of the photo-detector.

ELECTRICAL DESCRIPTION

The PD electronics are contained in a rectangular box mounted behind the image conduit. Figure 2 shows a block diagram of the signal processing performed by the PD circuitry. The IDP performs the functions of an optical detector and a current to voltage convertor. Its integral high gain and low output impedance minimize sensitivity to stray interference. AC coupling between amplifier stages removes the DC component of the optical signal introduced by ambient radiation levels and the interrogating LED beam. A video amplifier then amplifies the signal to a sufficiently high level to allow it to be compared with a reference threshold level of 25 mV. The circuit is edge coupled, in that the input signal is differentiated making the baseline-level independent of varying snow particle frequency and particle size. This permits comparison of the pulses with an absolute voltage level which represents a known beam intercept area. The assumption of edge coupling holds true to a snow particle frequency of approximately 3 kHz. Above this frequency the PD will still operate but with less precision. The data of Budd et al. (1966) and Schmidt (1982) suggest it is extremely unlikely that conditions which saturate the PD exist during blowing snow. No saturation has been observed

The comparator uses hysteresis to reduce the likelihood of noise on the signal generating multiple counts from a single snow particle interruption.

MASS FLUX CALCULATION

Theoretical considerations

The calculation assumes the optical properties of blowing snow particles may be modelled as ice spheres with a density equal to that of ice. Pomeroy and Male (1988) conclude this assumption is valid and use it to calculate the visual range in blowing snow from the drift density measurements of Budd et al. (1966), and compare the calculations to careful measurements of the visual range by Budd et al. The results indicate that modelling blowing-snow particles as ice spheres is a reasonable approximation for the PD.

Following Zuev (1970), the transmittance, τ, associated with a single spherical particle intercepting a collimated beam is found as:

$$\tau = \tau_0 - (r_p^2/r_b^2)Q_{eff} \qquad (1)$$

where τ_0 is the transmittance antecedent to the beam interception, r_p is the radius of the intercepting particle, r_b is the beam radius and Q_{eff} is the effective extinction efficiency. The difference between τ and τ_0 corresponds to the magnitude of the pulse height in the IDP signal.

The effective extinction efficiency is the ratio of radiant flux scattered and absorbed by a particle *so that it is not received by the detector* to that flux which actually intercepts the particle surface. Neglecting forward scattering from externally reflected radii (less than 0.1% of incident radiation for blowing snow particles), the effective extinction efficiency is equal to the particle extinction efficiency Q_e, less the correction due to detection of radiation diffracted forward by the particle ΔQ_d and

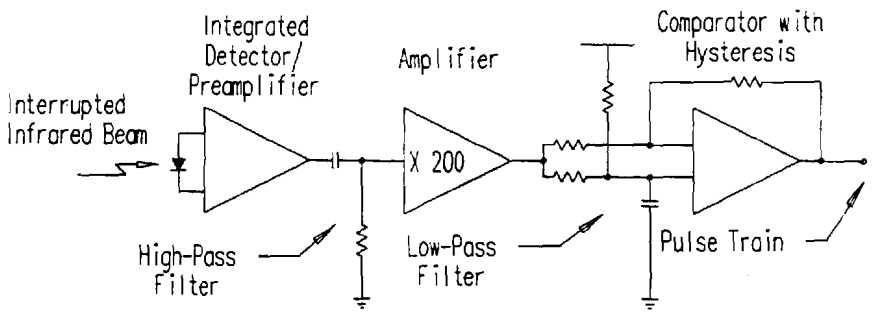

Fig. 2. Block diagram of particle detector signal processing.

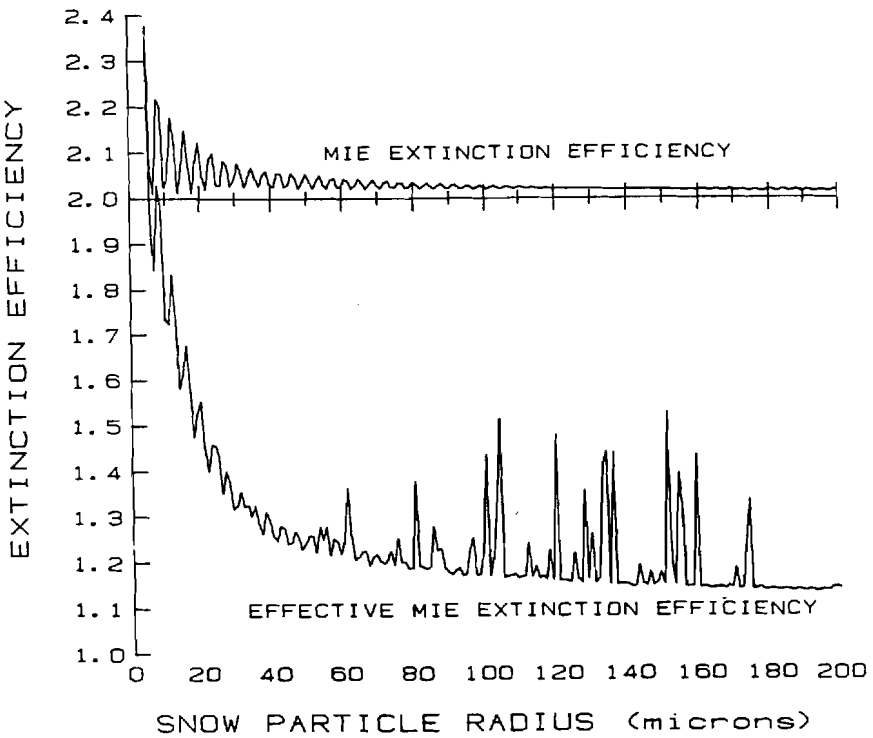

Fig. 3. Mie and Effective Mie extinction efficiency versus snow particle radius for the particle detector.

the correction due to detection of radiation refracted forward by the particle ΔQ_r, where:

$$Q_{eff} = Q_e - \Delta Q_d - \Delta Q_r \quad (2)$$

The extinction efficiency is a function of the particle radius and wavelength of radiation. For a mean wavelength of 820 nm it is best calculated from Mie theory (Mie, 1908) using the approximate Mie algorithm developed by Nussenzvieg and Wiscombe (1980). The extinction efficiency of ice spheres for a 50 nm band of radiation of mean wavelength equal to 820 nm is plotted against particle radii in Fig. 3. Wave-forms in the plot are due to interference between various orders of scattering rays. Q_e varies notably from the approximation of 2.0 used in some optics applications.

The diffraction correction to the extinction efficiency accounts for radiation diffracted forward by the particle into a solid angle defined by the detector radius r_b and distance l from particle to detector. Hodkinson and Greenleaves (1963) present a formula for ΔQ_d based upon the work of Van de Hulst (1957). Integrating this formula over the detection distance L, provides an average correction for the source-detector geometry:

$$\Delta Q_d = 1 - \int_0^L \{J_0^2[s \sin(r_b/l)] - J_1^2[s \sin(r_b/l)]\} dl \quad (3)$$

where $s = 2\pi r_i/\lambda$, λ is the mean wavelength and J_0 and J_1 are zeroth and first order Bessel functions of the first kind, respectively. For the PD, the magnitude of ΔQ_d can be 50% of Q_e and increases with particle radius.

The refraction correction ΔQ_r is a function of the complex index of refraction, n, and the particle/detector geometry. Integrating the formula presented by Hodkinson and Greenleaves (1963) over the detection distance provides:

$$\Delta Q_r = 4\left[\frac{n}{n^2-1}\right]^4 \int_0^\theta \frac{(nA-1)^3(n-A)^3(1+B)C}{A(n^2+1-2nA)^2} d\theta \quad (4)$$

where $A=\cos(\theta/2)$, $B=\sec^4(\theta/2)$, $C=\sin(\theta)$ and $\theta=\arcsin(r_d/l)$. ΔQ_r is much smaller than ΔQ_d for the optical geometry of the PD.

The calculated effective extinction efficiency for ice spheres in the PD is plotted with the extinction efficiency in Fig. 3. Q_{eff} is diminished by almost half as the particle radius increases from 10 to 50 μm. Interference phenomena are more evident in the effective extinction efficiency than the extinction efficiency because of forward diffraction, though irregularies in particle shape are likely to average these effects somewhat.

Calculating Q_{eff} without integrating over distance L provides the transmittance associated with an intercepted particle radius and its variation with particle crossing position between the source and detector. Equation 1, the Mie algorithm, Eq. 2, 3 and 4 calculate the transmittance τ for the PD beam geometry as a function of the radius of the particle and l; the results are plotted in Fig. 4. The blowing snow particles extinguish less radiation as distance to the detector decreases. This effect becomes most severe very near to the detector. Inconsistencies in some values for τ (especially for large particles) result from diffraction interference effects, which average out when a range of particle sizes is considered.

For a threshold transmittance of detection $\tau_d=1.0$ and particle radii much less than the beam radius, and interruptible length L, the sampling area of the detection beam is:

$$A_s=2Lr_b \tag{5}$$

If the number of particles counted by the detector per unit time is ϕ, then the number flux, F_p, of snow particles through a unit area of the atmosphere normal to the flux is,

$$F_p=\phi\ /A_s \tag{6}$$

Owing to practical considerations τ_d has a value less than one. Hence only snow particles with an ef-

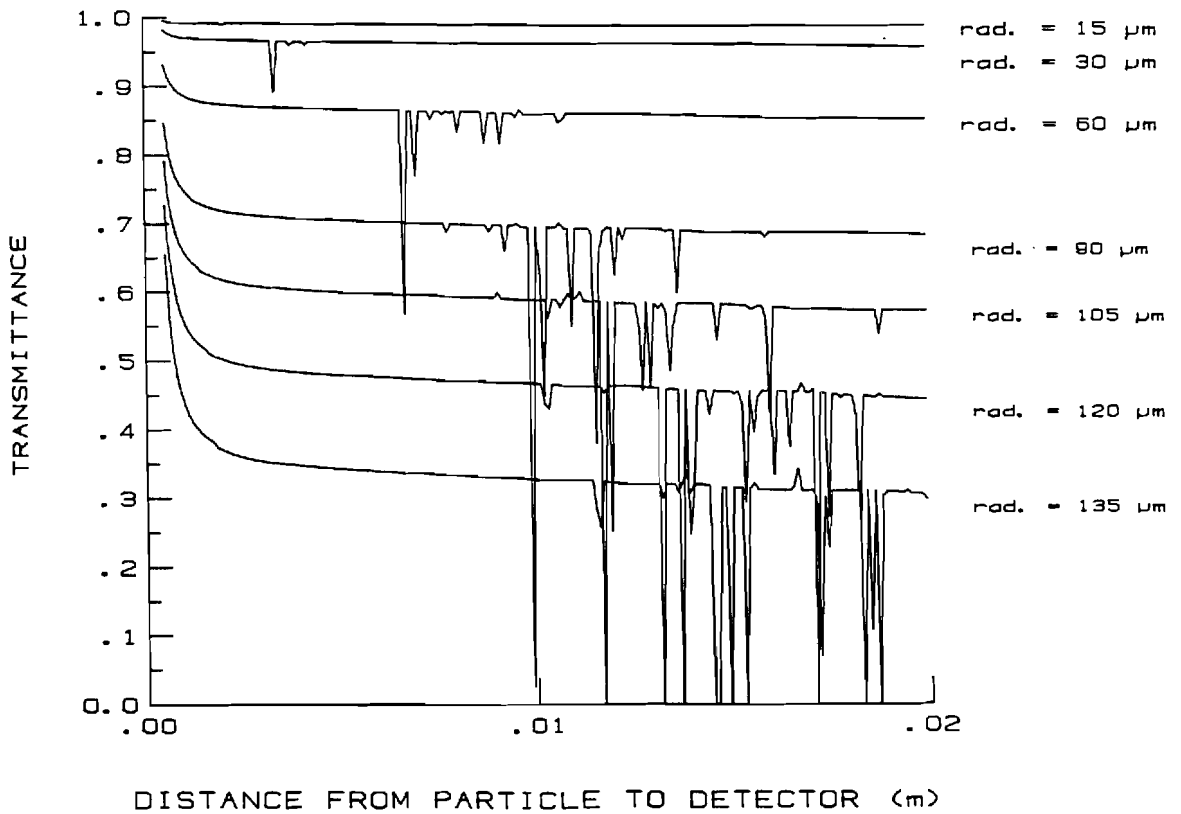

Fig. 4. Radiative transmittance versus distance from the particle to the detector for a range of particle radii.

fective area greater than the threshold area A_d will cause the transmittance to fall below the threshold level and be counted, that is snow particles with radii greater than r_d assuming spherical snow particles.

The PD beam cross-sectional radius is of the same order of magnitude as that of a larger snow particle. A large particle can have a path which only partially intercepts the detection beam and still have an intercept area greater than the threshold area. Thus the sampling area of the beam varies with the size of particle and Eq. 5 becomes:

$$A_s = 2LG \tag{7}$$

where G is the perpendicular distance between the snow particle centre and the centre of the detection beam when the overlap area is equal to the threshold area. G is found from a consideration of particle and beam geometry. The threshold radius for detection is related to G via the expression:

$$A_d = r_p^2[X - \sin(X)] + r_b^2[Y - \sin(Y)] \tag{8}$$

where:

$$X = 2\arccos\left[\frac{G^2 + r_p^2 - r_b^2}{2Gr_p}\right] \tag{9a}$$

and:

$$Y = 2\arccos\left[\frac{G^2 + r_b^2 - r_p^2}{2Gr_b}\right] \tag{9b}$$

G is found from the beam radius, particle radius and threshold area for detection using an iterative solution.

To calculate the flux of particles from PD measurements, Eq. 6 is modified for: (1) not counting particles with an effective area less than the threshold area: and (2) varying sampling area with particle size. To account for the threshold area of detection, the number density of particles with size greater than the threshold for detection is divided by the cumulative frequency of particles of size greater than the threshold. To account for the sampling area being a function of radius, the frequency of each assumed snow particle radius is divided by the corresponding sampling area. The gamma distribution (Budd, 1966) describes the frequency distribution of blowing snow particle radii where:

$$f(r_p) = \frac{r_p^{(\alpha-1)} e^{(-r_p/\beta)}}{\beta^\alpha \Gamma(\alpha)} \tag{10}$$

and $f(\ )$ denotes the frequency, Γ is a gamma function and α is the shape parameter and β is the scale parameter of the gamma distribution. The resulting expression for F_p, corrected for the sampling area of each particle size using the gamma distribution to calculate the frequency of particle radii, is:

$$F_p = \frac{\phi \int_{r_d}^{\infty} r_p^{(\alpha-1)} e^{(-r_p/\beta)} A_s^{(-1)} dr_p}{\int_{r_d}^{\infty} r_p^{(\alpha-1)} e^{(-r_p/\beta)} dr_p} \tag{11}$$

The mass flux of blowing snow through a differential area, q, is found by multiplying the number flux of particles by their mass. The gamma distribution describes the distribution of particle radii, hence the mass flux of blowing snow particles is:

$$q = \frac{4\pi\rho_p F_p}{3\beta^\alpha \Gamma(\alpha)} \int r_p^{(\alpha+2)} e^{(-r_p/\beta)} dr_p \tag{12}$$

where ρ_p is the blowing snow particle density (assumed equal to that of ice, see Pomeroy and Male, 1988) and Γ denotes a gamma function.

Mass flux calculation for blowing snow

The linearity of the PD was checked using a spinning wire which was moved across the measuring throat of the gauge normal to the beam, from the LED to the image conduit. Little variation in the PD output signal was found.

From the diameter of the spinning wire and its angular velocity the effective radius of the detection beam was determined to be approximately 170 μm, differing slightly from the pinhole radius.

By superimposing small current pulses on the normal LED drive current, the absolute threshold level of each gauge is set to a threshold transmittance $\tau_d = 0.9765$. This is the maximum performance attainable from the electronics. The blowing snow particle radius equivalent to this threshold transmittance can be found from Eq. 1 by proceeding from an initial value of Q_{eff} selected from Fig. 3. Using $r_b = 170$ μm, r_d has a value of 22.5 μm. Solv-

ing Eq. 8 and 9 iteratively, G is fitted to a power-law function of r_p, giving:

$$G=0.007131r_p^{0.356} \quad (13)$$

with a coefficient of determination, R^2 of 0.99; note that both variables are in metres. As $L=0.02$ m, the sampling area is a function of the particle radius being sampled:

$$A_s=0.0002852r_p^{0.356} \quad (14)$$

again both variables are in metres.

Equations 11 and 12 relate the number of particles counted by the PD to the mass flux, if assumptions are made regarding the values of α and β which comprise the particle size distribution. The blowing snow measurements of Budd (1966) and Schmidt (1981, 1982) provide suitable values for these variables, specific to ranges of heights above the surface. For the layer of saltating blowing snow particles, defined for measurements at heights less than 0.05 m, $\alpha=5$ and $\beta=2\times10^{-5}$ m, yields $\bar{r}_p=100$ μm (Schmidt, 1981). For the layer of suspended blowing snow particles below 1 m height and above 0.04 m height, $\alpha=10$ and $\beta=6\times10^{-6}$ m, yields $\bar{r}_p=60$ μm (Budd, 1966; Schmidt, 1982). For suspended blowing snow above 1 m height $\alpha=15$ and $\beta=2.66\times10^{-6}$ m, yielding $\bar{r}_p=40$ μm (Budd, 1966). Using these values for α and β the following relationships between flux and PD counts are determined:

(a) for the saltation layer:

$$q=617\times10^{-6}\phi \quad (15)$$

(b) for the suspended layer below 1 m height:

$$q=122.8\times10^{-6}\phi \quad (16)$$

and (c) for the suspended layer above 1 m height:

$$q=40.23\times10^{-6}\phi \quad (17)$$

Note that q is the mass flux through a differential area normal to the flow at the height of the gauge beam centre above the surface in units of kg/m^2 s and ϕ is the number of particles counted by the gauge per second.

FIELD TESTS

Seven PDs were operated continuously over the winters of 1985–86 and 1986–87 at sites in south-central Saskatchewan, Canada. Temperatures during the measurements ranged from -39°C to $+2$°C and wind speeds exceeded 20 m/s. The gauge operated normally throughout these conditions. The only maintenance required involved uncovering instruments buried by saltating snow. The optical components remained frost and ice-free, except for one day with freezing rain and blowing snow.

To permit an evaluation of the PD and the mass flux calculation procedure, the PD was operated alongside a small filtre-fabric drift trap. The filtre-fabric trap has a rectangular orifice with dimensions of 20×150 mm with a "sock" of 0.105 mm mesh filtre-fabric extending 380 mm behind the orifice. The trap is mounted on a swivel and orients into the wind. While the efficiency and accuracy of the trap is not known precisely, it has been used to evaluate Gubler's (1981) and Schmidt's (1984) blowing snow particle counters and may thus be considered a "standard" for comparison. A full description of the filtre-fabric trap is presented by Schmidt et al. (1984).

The evaluation was conducted at a level site 50 km west of Laramie, Wyoming, U.S.A., during a severe blowing snow-storm on 11 Feb., 1988. Wind speeds were as high as 30 m/s at 1 m height during this event. Both the filtre-fabric trap and the PD were maintained at 0.37 m above the snow surface. For this experiment, the PD output was accumulated continuously and the counter recorded and reset every 10 s. The snow accumulation in the filtre-fabric trap was weighed after collection periods ranging from 2 to 9 min. Table 1 lists the mass fluxes calculated by Eq. 16 (PDF) and the corresponding fluxes measured by the filtre-fibre trap (FFF). The mean difference (PDF$-$FFF) of 0.00211 kg/m^2 s suggests the differences are not systematic although there is a minor trend for the PDF values to be greater than the FFF at the larger fluxes. A relatively-large standard deviation of the difference of 0.03457 kg/m^2 s is attributed to measurement errors and wide variations in wind velocity and concentration of wind-transported snow between sam-

TABLE 1

Estimates of blowing snow flux in kg/m^2 s at 0.37 m height, Laramie Plains, Wyoming on 11 February, 1988

Filtre-fabric mass flux is calculated from snow accumulations in the trap, weighed after a known exposure time; PD mass flux is calculated from the number of counts occurring during the same time period; exposure times are in the range of 2–9 min

PD mass flux	FF mass flux	Difference
0.038	0.05109	−0.01259
0.0561	0.9799	−0.04189
0.062	0.05395	0.00805
0.0667	0.08957	−0.02287
0.09074	0.12632	−0.03558
0.1089	0.09105	0.01785
0.1609	0.11642	0.04448
0.1947	0.13527	0.05943
Mean		0.00211
Standard deviation		0.03457

pling points. Unfortunately, the small number of data do not permit derivation of a strong relationship between the two estimates. The correspondence between the PD fluxes with the trap fluxes is, however, good or better than those reported by Schmidt et al. (1984) for a number of different particle counters and mass flux computation procedures.

CONCLUDING COMMENTS

The PD counts the number of particles passing through a narrow beam of radiation; the flux of blowing snow is estimated from this measurement. The output of the gauge is sensitive to the optical properties of the blowing snow particles, their density and the size of particles. Mie electromagnetic scattering theory and other radiation scattering calculations provide a means to relate the PD output to blowing snow flux.

The PD is suitable for determining the mass flux of blowing snow over the range of wind-speeds, temperatures and ambient light levels common to wind-swept locations possessing moderate to severe continental climates.

ACKNOWLEDGEMENTS

The authors received support from Natural Sciences and Engineering Research Council of Canada Operating Grant No. A4363 and the Saskatchewan Research Council. The assistance of Dr. R.A. Schmidt, Rocky Mountain Forest Range Experiment Station, Fort Collins, Colo., U.S.A., with field data collection, logistics and data retrieval in Wyoming is gratefully acknowledged. The support and guidance of Dr. D.M. Gray, Division of Hydrology, in the development of the PD, is very much appreciated.

REFERENCES

Budd, W.F., 1966. The drifting of non-uniform snow particles. Studies in Antarctic Meteorology. Am. Geophys. Union, Antarct. Res. Ser., 9: 59–70.

Budd, W.F., Dingle, W.R.J. and Radok, U., 1966. The Byrd snow drift project: Outline and basic results. Studies in Antarctic Meteorology. Am. Geophys. Union. Antarct. Res. Ser., 9: 71–134.

Gubler, H., 1981. An electronic remote snow-drift gauge. J. Gaciol., 27 (95): 164–174.

Hodkinson, J.R. and Greenleaves, I., 1963. Computations of light-scattering and extinction by spheres according to diffraction and geometrical optics, and some comparisons with the Mie theory. J. Opt. Soc. Am., 53 (5): 577–588.

Mie, G., 1908. Beitrage zur Optik truber Medien. speziell Kolloidalen Metalllosungen. Ann. Physik, 25: 377–445.

Nussenzvieg, H.M. and Wiscombe, W.J., 1980. Efficiency factors in Mie scattering. Phys. Rev. Lett., 45 (18): 1490–1494.

Pomeroy, J.W. and Male, D.H., 1988. Optical properties of blowing snow. J. Glaciol., 34 (116): 3–9.

Schmidt, R.A., 1977. A system that measures blowing snow. U.S. Dep. Agric., For. Serv. Res. Pap., RM-194. 33 pp.

Schmidt, R.A., 1981. Estimates of threshold windspeed from particle sizes in blowing snow. Cold Reg. Sci. Technol., 4: 187–193.

Schmidt, R.A., 1982. Vertical profiles of wind speed, snow concentration and humidity in blowing snow. Boundary-Layer Meteorol., 23: 223–246.

Schmidt, R.A., 1984. Measuring particle size and snowfall intensity in drifting snow. Cold Reg. Sci. Technol., 9: 121–129.

Schmidt, R.A., Meister, R. and Gubler, H., 1984. Comparisons of snow drifting measurements at an alpine ridge crest. Cold Reg. Sci. Technol., 9: 131–141.

Van de Hulst, H.C., 1957. Light Scattering by Small Particles. Wiley, New York, N.Y., 470 pp.

Zuev, V.E., 1970. Propagation of Visible and Infrared Radiation in the Atmosphere (Transl. D. Lederman). Israel Programme Sci. Transl., London, 405 pp.